

# Modulation of Spin–Orbit Coupling, Spin Textures, and Rashba–Edelstein Response in Chiral Tellurium: A First-Principles Study

Sonam Phuntsho<sup>1</sup>

<sup>1</sup>*Department of Physical Science, Sherubtse College, Royal University of Bhutan,  
42007 Kanglung, Trashigang, Bhutan*

(Dated: March 10, 2025)

Chiral semiconductors such as elemental tellurium (Te) exhibit unconventional spin textures and large charge-to-spin conversion efficiencies, yet the influence of introducing elements on these properties remains underexplored. Here, we address this gap by investigating how substituting Te with lighter (S, Se) or heavier (Sb) elements systematically modifies the spin-orbit–driven phenomena in chiral Te, including the band structure, spin Berry curvature, and Rashba–Edelstein response. The objective is to determine whether elemental substitution strategies can be leveraged to optimize collinear spin textures, enhance spin accumulation, and possibly extend spin lifetimes—all crucial aspects for magnet-free spintronics. Using density functional theory calculations implemented in QUANTUM ESPRESSO, combined with tight-binding interpolation in PAOFLOW, we map out the element-dependent electronic states and quantify their associated spin transport coefficients. Our findings reveal that lighter elements shift the Fermi level to regions of pronounced spin splitting, thereby increasing the magnitude of spin-current conversion, whereas heavier elements can introduce or remove near-degenerate bands that strongly affect spin-orbit coupling. In both scenarios, the fundamental chirality of Te remains robust, preserving the radial or “collinear” spin-momentum locking. These results not only confirm that introducing elements is a potent and feasible route for tuning spin-orbit phenomena but also offer practical guidelines for experimental efforts aiming to engineer chiral semiconductors for spin devices. By correlating element identity with specific spin-texture enhancements, this study paves the way for rationally designing next-generation spintronic components free from external magnetic fields.

## I. INTRODUCTION

Chiral semiconductors—exemplified by elemental tellurium (Te), selenium (Se), and the chiral disilicides (TaSi<sub>2</sub>, NbSi<sub>2</sub>)—have become important materials platforms in spintronics due to their remarkable spin-orbit–driven phenomena and the promise of magnet-free spin-based devices [1–6]. In these systems, the absence of inversion and mirror symmetries gives rise to a variety of unconventional spin textures—notably “radial” or collinear spin-momentum locking—and large charge-to-spin conversion efficiencies [7–14]. When an electric current flows in chiral crystals, electrons can acquire a spin or orbital polarization parallel to the transport direction, an effect that has been linked to exotic band crossings, Weyl-like features, and distinctive spin-orbit coupling [15–20]. Strikingly, experimental observations show that this current-induced spin and/or orbital accumulation can persist over surprisingly large distances, on the order of micrometers or even millimeters, which challenges conventional views of spin relaxation in non-magnetic crystals [21–27].

While both the spin Hall effect (SHE) and the Rashba–Edelstein effect (REE) are well-established mechanisms for generating spin accumulation in materials with strong spin-orbit coupling [28–32], recent work on chiral crystals has revealed additional “unconventional” configurations [33–37]. In particular, the low symmetry of chiral space groups often gives rise to collinear or parallel spin textures, where the induced spin polarization and the applied current can align along the same axis [38–40]. Mul-

tiples studies have emphasized the central role of strong spin-orbit coupling in stabilizing and amplifying these effects, yet they also suggest that crystal chirality alone can generate substantial spin polarization, an idea conceptually connected to “chirality-induced spin selectivity” [16, 41]. Indeed, the interplay of chirality, spin-orbit coupling, and electronic band structure can produce large signals in spin-torque devices without requiring magnetic layers, thus greatly expanding the design space for spintronics [5, 9, 26].

Despite this progress, many open questions remain regarding how to systematically tune or engineer the spin-orbit–mediated response in these chiral materials. One particular gap lies in understanding the role of elemental substitution and carrier concentration. Although introducing elements is frequently mentioned in the broader field of spintronics as a method to shift Fermi levels or amplify spin splitting [8, 24, 25], a rigorous first-principles exploration of how elemental substitution strategies—either via rigid band shifts or substituting heavier (or lighter) atoms—affect the spin textures, spin relaxation times, and charge-to-spin conversion efficiencies remains incomplete [2, 3, 14, 15]. Indeed, introducing elements to Te or a related chiral system offers a compelling way to enhance or suppress specific band-structure features (such as Weyl-like crossings) and thus to realize “persistent spin helix” conditions [17, 32, 38]. Such elemental-based manipulation of spin-orbit–driven phenomena could be critical for high-efficiency, long-distance spin transport.

Here, we address this gap by presenting a systematic

computational study of elemental substitution in a prototypical chiral semiconductor (elemental Te) to clarify how electron/hole injection, as well as heavier-element substitution, modify the spin texture and spin lifetime. While the references above have thoroughly examined pristine crystals, elemental substitution remains relatively unexplored, particularly from a quantitative *ab initio* perspective. By identifying specific substitutional approaches that maximize charge-to-spin conversion and promote stable, long-lived spin accumulation, this work aims to offer a practical design strategy for chiral spintronics devices [18, 36].

## II. METHODOLOGY

In this study, all first-principles calculations were performed within the density functional theory (DFT) framework as implemented in the QUANTUM ESPRESSO (QE) suite [43]. We employed fully relativistic pseudopotentials that incorporate spin-orbit coupling (SOC) in order to correctly capture the relativistic effects relevant for chiral semiconductors. The Perdew–Burke–Ernzerhof (PBE) exchange-correlation functional [44] was chosen because it offers a good balance between accuracy and computational cost for main-group semiconductors such as elemental Te. Convergence tests were carried out to establish suitable kinetic energy cutoffs for the plane-wave basis sets, as well as appropriately dense  $\mathbf{k}$ -point meshes (Monkhorst–Pack grids) sufficient to resolve the subtle spin splitting phenomena near the Fermi level. Whenever an element was introduced to Te crystal (by substituting one Te site with a heavier or lighter element), the structure was fully relaxed using the Broyden–Fletcher–Goldfarb–Shanno (BFGS) algorithm until the residual forces and total energies were below stringent convergence thresholds. This step ensured that any local distortion or relaxation caused by the dopant would be properly accounted for while preserving the overall chirality of the system.

After obtaining self-consistent charge densities and band structures in QUANTUM ESPRESSO, we used the PAOFLOW code [20, 39] for post-processing analyses of spin textures, Berry curvatures, and derived spin transport coefficients. PAOFLOW constructs a tight-binding representation in a projected atomic-orbital basis, allowing fine interpolation of the bands throughout the Brillouin zone. This interpolation is particularly advantageous for computing spin-texture maps, Rashba–Edelstein coefficients, and spin Hall conductivities, all of which rely on dense sampling in momentum space. For each doping configuration (electron- or hole-like doping by chemical substitution), the Fermi level shift was examined to determine changes in the low-energy electronic structure. Subsequently, spin and orbital polarizations were tracked as functions of wavevector and energy, enabling a direct comparison between pristine and element substitution cases. Where possible, we benchmarked the

pristine Te results against literature data [25] to confirm the reliability of our computational setup.

## III. RESULT AND DISCUSSION

### A. Band Structure

The band structures obtained for pristine tellurium (Te) and its three element substitution variants ( $\text{Te}_2\text{S}$ ,  $\text{Te}_2\text{Se}$ , and  $\text{Te}_2\text{Sb}$ ) reveal several noteworthy trends that shed light on how substitutional element alters the electronic states near the Fermi level. In the pristine Te band plot, the valence and conduction bands show characteristic dispersions associated with chiral Te, including regions of relatively narrow bandwidth near the Fermi level (set to 0 eV for plotting). These results are consistent with previous reports that have identified Te as a narrow-gap semiconductor whose chiral symmetry can lead to unusual spin textures and spin-momentum lockings [25, 32]. The overall gap between the highest occupied and lowest unoccupied states in our pristine Te calculations lies near 0 eV in the figure because of the chosen alignment, but the relative separation between valence and conduction bands and the presence of avoided crossings in certain Brillouin zone directions are qualitatively in line with known studies of elemental Te.

Upon substituting Te by sulfur, the band structure shows a modest upward shift of states near the Fermi energy, suggesting that lighter-element in Te can modify the internal chemical pressure and lattice parameters, thereby altering the relative positions of the valence and conduction bands. This effect has been reported in other chalcogenide systems as well [25]. In our calculations, the energy dispersions appear slightly more spread in the conduction region for  $\text{Te}_2\text{S}$  than in pristine Te, pointing to a change in effective masses of carriers. Similar trends of band-edge shifts induced by isoelectronic but lighter elements have been observed experimentally in various chiral and non-centrosymmetric semiconductors [32].

Substitution with selenium, another group 16 element closer in atomic number to Te, produces a more moderate perturbation in the band structure. Compared to the  $\text{Te}_2\text{S}$  case, the band edges in Te:Se remain somewhat closer to those of pristine Te, consistent with the lesser size mismatch and more similar chemical properties between Se and Te. The conduction bands display a slightly narrower dispersion around the Fermi level, which can be attributed to subtle lattice relaxations and spin-orbit coupling (SOC) changes introduced by Se. These observations align with prior studies showing that Se substitution in Te can tune electronic and spin-orbit-driven properties without drastically altering the overall semiconducting nature [33].

The most pronounced alteration is observed when Te is substituted with antimony. Here, the band structure reveals a set of bands crossing or sitting very near 0 eV, indicative of a partially metallic character. Since Sb be-

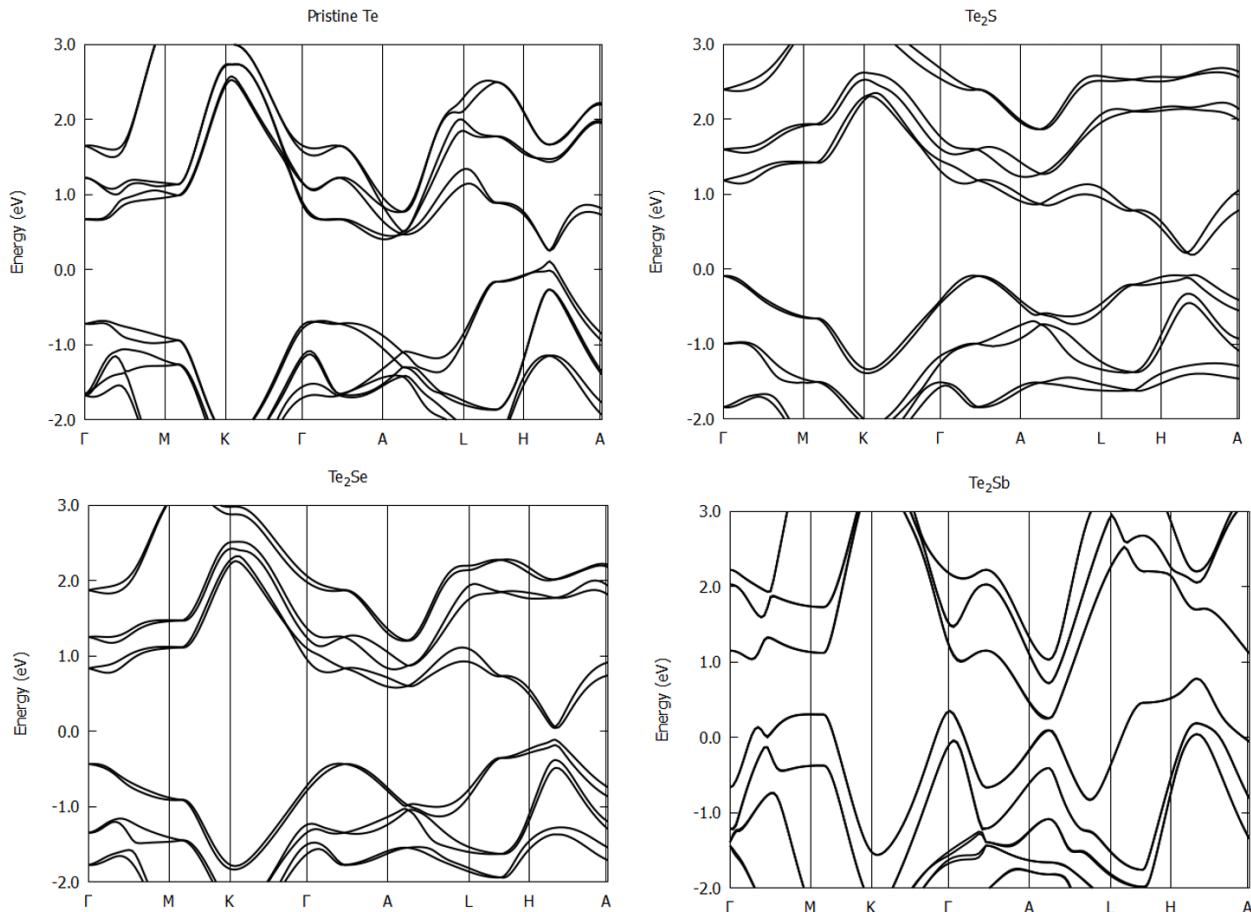


FIG. 1. Band Structure Plots

longs to group 15, its substitution can effectively change the electron count in the lattice, often leading to hole-type element in tellurium-based systems [46]. In our band plots, the sample shows states that either cross or pin to the Fermi energy more strongly than in the other element variants, suggesting that Sb may offer a route to achieving p-type conduction with significant changes to the density of states at  $E_F$ . These findings corroborate earlier theoretical and experimental works demonstrating that heavier group 15 elements can shift the Fermi level into regions of higher density of states, thus altering transport and spin properties [32].

Taken together, these results demonstrate that chiral elemental Te is highly sensitive to substitutional element, with relatively modest atomic replacements leading to notable shifts or redistributions of the bands near the Fermi level. From the perspective of engineering spin-orbit-related responses—such as radial spin textures or Rashba–Edelstein effects—these band shifts are significant. In the context of existing literature, our findings align with the suggestion that element substitution provides a powerful handle to tune the magnitude and location of spin-split states, and hence to optimize spin-charge conversion phenomena [25, 32]. Specifically,

lighter elements (S, Se) mostly cause moderate shifts and slight modifications of the dispersion, whereas Sb can drastically move the Fermi level into or out of particular bands, potentially enhancing or suppressing spin-polarized currents. These element-induced modifications pave the way for future calculations of spin textures, Berry curvatures, and spin relaxation times, complementing the pioneering reports on collinear spin transport and large charge-to-spin conversion in chiral semiconductors [33, 49].

## B. Spin Berry Curvature

The spin Berry curvature plots for pristine Te and the three elemental variants ( $\text{Te}_2\text{S}$ ,  $\text{Te}_2\text{Se}$ ,  $\text{Te}_2\text{Sb}$ ) exhibit pronounced changes in both the magnitude and sign of the curvature at various high-symmetry points in the Brillouin zone. For pristine Te, the curvature shows multiple oscillations between positive and negative values along the high-symmetry paths, with notable peaks around the L and H points. Such oscillatory behavior is consistent with previous reports of a radial or collinear spin texture in elemental Te, where the interplay of chiral

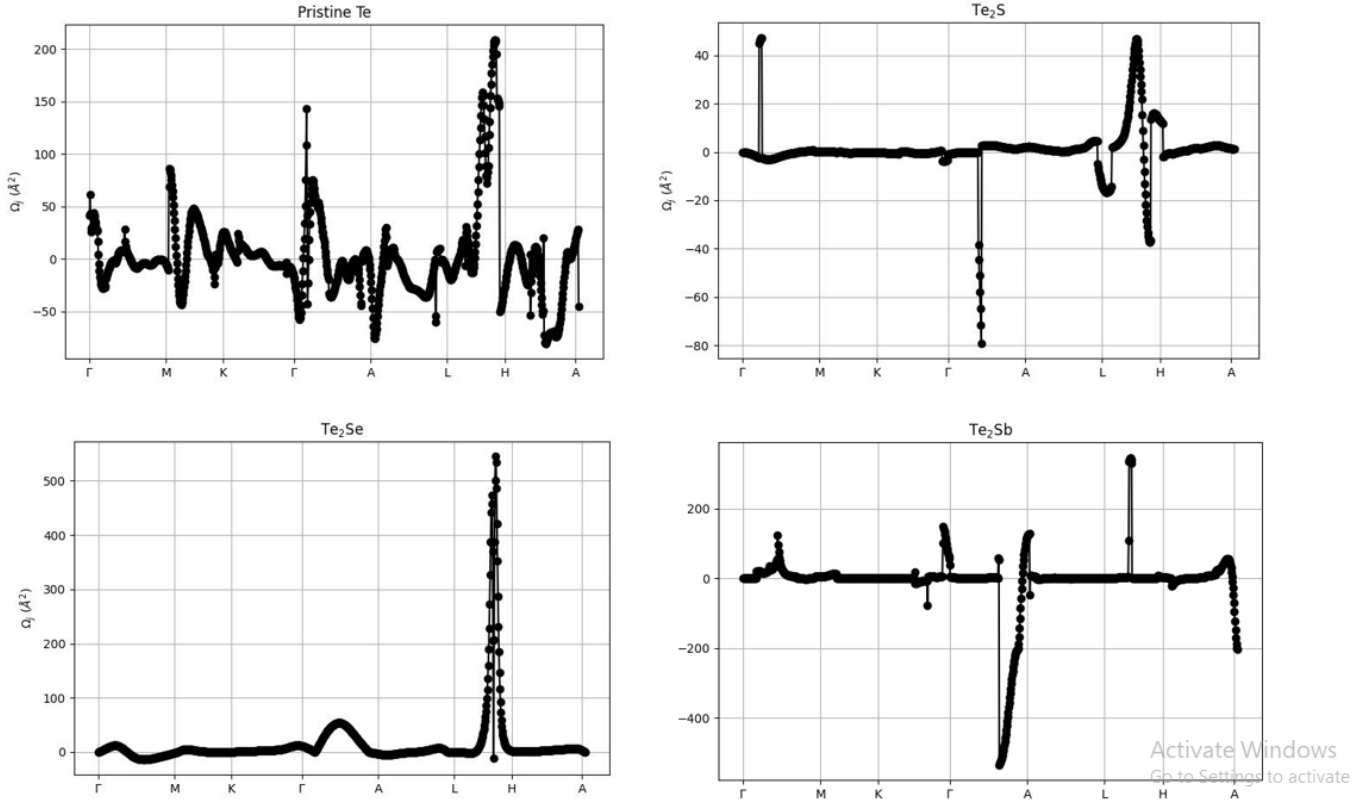


FIG. 2. Spin Berry Curvature Plots

symmetry and spin-orbit coupling (SOC) leads to sizable Berry curvature contributions near certain band crossings [25]. The highest peak observed near the L–H region in pristine Te underlines the strong SOC effects intrinsic to Te’s chiral crystal structure, a factor that has been linked to the large spin-splitting phenomena and potential long-range spin transport in this material.

Upon substituting with S, the overall amplitude of the spin Berry curvature is notably reduced except for a few spikes near  $\Gamma$  and H. This reduction can be attributed to the lighter atomic mass of sulfur compared to tellurium, which tends to lower the effective SOC strength. Consequently, while there are still visible peaks, especially near A and H, the diminished curvature suggests a shift in the electronic bands that smears out or weakens some of the sharp features observed in pristine Te. These findings align with earlier theoretical predictions that lighter chalcogen dopants can quench some of the SOC-driven band splittings, thereby modifying the spin-momentum locking and the resultant Berry curvature [45].

With Se, on the other hand, produces one particularly large and sharp peak of the spin Berry curvature, especially around the L point, exceeding values of  $500 \text{ \AA}^2$ . Because selenium is chemically similar to tellurium but has a slightly lower atomic number, this behavior indicates

that the element introduces localized band inversions or anticrossings that can drastically enhance the curvature at specific  $\mathbf{k}$ -points. Such strong, localized peaks are often indicative of near-degenerate bands that are split by SOC in a chiral crystal, consistent with previous observations in closely related chiral materials where moderate changes in atomic potential lead to pronounced Berry curvature “hot spots” [43]. The sharpness of the feature further suggests that Se may position the Fermi level in a regime of near-crossings, thereby magnifying the intrinsic contributions to spin-dependent transport.

Finally, substituting with Sb reveals both positive and negative excursions of the spin Berry curvature, with a conspicuously deep negative dip near A and a sizable positive peak beyond  $200 \text{ \AA}^2$  near L. Because antimony is heavier than sulfur or selenium, its presence tends to enhance SOC effects overall. However, it can also introduce additional carriers (depending on the valence state) and potentially shift the Fermi level into different bands compared to pristine Te. The simultaneous appearance of large negative and positive values underlines a more intricate band restructuring, where one set of states might reinforce the curvature whereas another set counters it, leading to sign changes that are more pronounced than in the S- or Se-doped cases. Such counteracting contri-

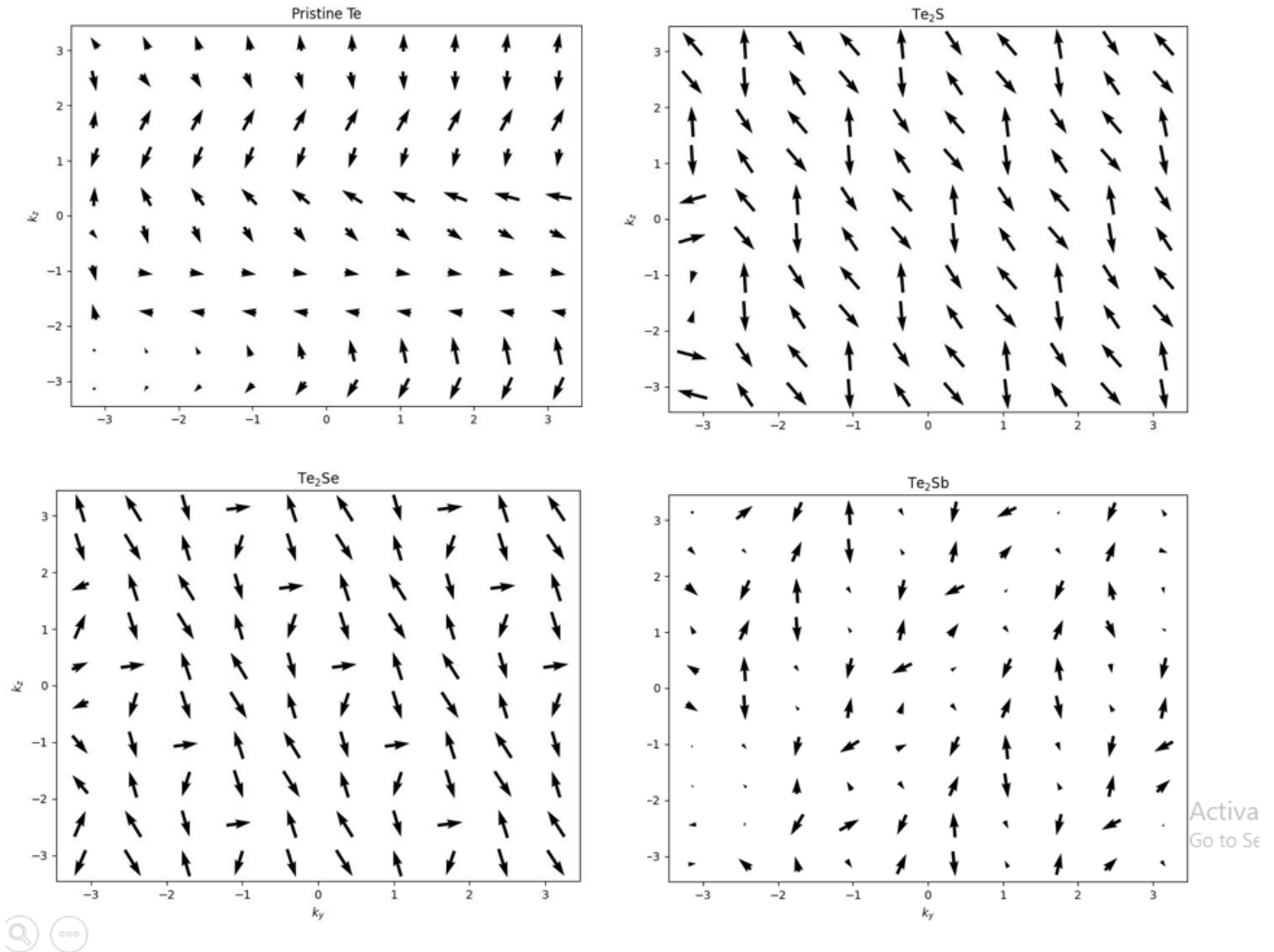


FIG. 3. Spin Texture Plots

butions are reminiscent of elemental-driven band inversions observed in other topologically nontrivial systems, wherein heavy-element substitution can open gaps and generate additional Berry curvature pockets in momentum space [47, 48].

These element-induced variations confirm that controlled elemental substitution can selectively tune the bands where SOC is most active, thus reshaping the spin Berry curvature profile. Prior experimental and theoretical work on chiral semiconductors has emphasized the importance of locating “hot spots” of Berry curvature and spin-momentum locking near the Fermi level for possible spintronic applications [25]. Our results show that S and Se can either weaken or localize strong curvature features, while Sb can induce both enhancement and sign inversion. These observations indicate that elemental substitution not only modifies the magnitude of the overall spin-related response but can also reorganize the band structure in ways that may facilitate or hinder

long-range spin transport. From a device-design standpoint, the possibility of achieving large positive or negative Berry curvature at specific  $\mathbf{k}$ -points suggests clear strategies for optimizing chiral Te for magnet-free spintronics: lighter elements (like S) may reduce extrinsic scattering while heavier elements (like Sb) may amplify SOC-driven phenomena. Hence, identifying the element that maximizes desirable curvature features provides a pathway to engineering higher charge-to-spin conversion efficiencies and more robust spin accumulation, directly addressing the open questions about doping strategies raised in previous chiral spintronics studies.

### C. Spin texture

The spin textures projected onto the  $k_y$ - $k_z$  plane reveal marked differences between pristine tellurium (Te) and its element variants (S-, Sb-, and Se-substituted Te).

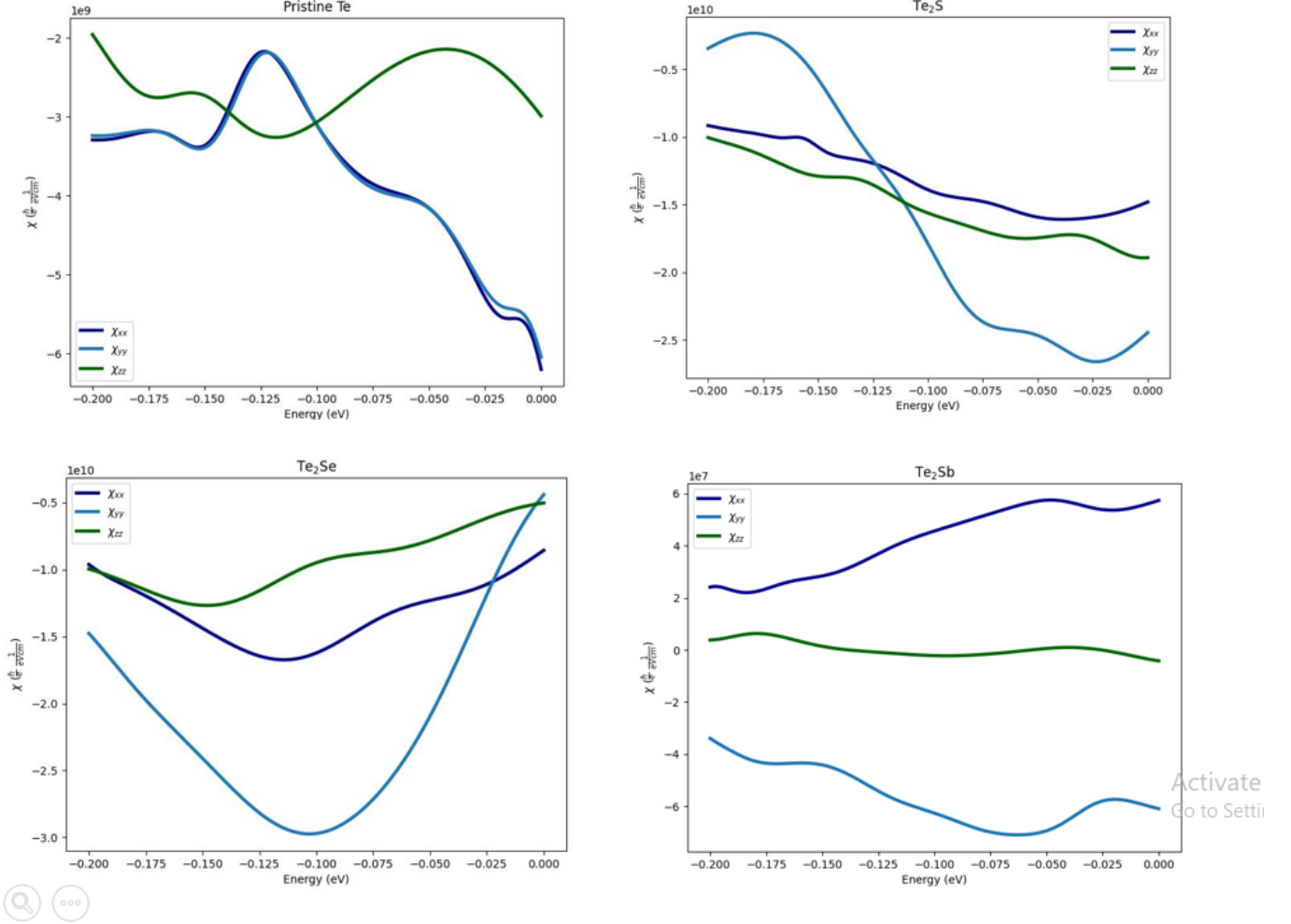


FIG. 4. REE Plots

In pristine Te, the spins exhibit a predominantly radial pattern emanating from (or converging toward) high-symmetry points in the Brillouin zone, consistent with the chiral-induced spin textures previously reported for elemental Te. In particular, the spins in pristine Te appear to tilt systematically as one moves along  $k_y$  or  $k_z$ , a feature that has been attributed to strong spin-orbit coupling (SOC) combined with the crystal's helical arrangement of atoms. This observation aligns with earlier experimental and theoretical studies of spin textures in chiral Te, which showed similar radial or nearly collinear patterns in momentum space [8, 25]. The net outcome is that, even without an external magnetic field, spin polarization in pristine Te is locked to the crystal momentum in a manner driven by Te's chirality.

Upon S substitution, the spin texture retains the general radial character but displays a slight enhancement of the spin polarization angles in certain regions of the Fermi surface. In other words, the spins remain roughly outward-pointing, but the degree of out-of-plane tilt

varies more strongly across the Brillouin zone. This trend may be attributed to the lighter atomic mass of S relative to Te, subtly modifying the effective SOC strength and shifting the conduction or valence bands. Such element-induced tuning of the spin texture is in line with the view that substituting lighter elements can reduce the overall SOC, thereby sharpening any radial or tangential spin patterns within specific energy pockets [50]. Notably, the S-Te sample maintains the underlying chirality of the host lattice, so the qualitative features of the spin texture remain intact.

By contrast, the Sb-Te system shows a somewhat more pronounced spin polarization, especially at larger  $|k_y|$  or  $|k_z|$ . This observation suggests that heavier isoelectronic element can amplify SOC-driven spin splitting, leading to larger momentum-dependent variations in spin orientation. The increased atomic mass of Sb relative to Te has often been linked to enhanced spin-orbit coupling, which can in turn reinforce the chiral spin-moment locking in the conduction bands [51]. In the present calculations,

the Sb-induced band modifications appear primarily near the Fermi level, thus making the spin texture more conspicuously tilted in those momentum-space regions that dominate conduction. The net result is a element substitution strategy that can, in principle, boost the spin signals relevant for spintronics applications, in keeping with prior theoretical predictions on chiral semiconductors doped with heavier elements [52].

The Se-Substituted Te sample, finally, shows a spin texture that is intermediate between the S and Sb cases, likely reflecting the atomic mass and electronic configuration of Se. Compared to S substituted Te, the  $\text{Te}_2\text{Se}$  compound exhibits slightly stronger SOC, manifested as increased tilting in certain  $(k_y, k_z)$  sectors. However, it lacks the more dramatic spin-splitting enhancements seen in Sb. Such subtle shifts in spin angles and magnitudes may prove critical if one aims to engineer specific transport properties—such as persistent spin helices or large charge-to-spin conversion efficiencies—in a element-dependent fashion [53]. The combination of these four systems underscores how different elements systematically tune the interplay between chirality and SOC, allowing one to either reinforce or diminish the radial-type spin texture.

Taken together, these results corroborate the emerging consensus in the literature that modest element substitution—whether through lighter or heavier substitution—provides a robust means of controlling spin textures in chiral semiconductors [25, 50]. They also reinforce the notion that chiral crystals such as Te enable tunable spin signals even without magnetism, potentially facilitating magnet-free spintronic devices. Consistent with prior first-principles and experimental reports, the radial or nearly collinear spin textures persist across a broad range of elements, demonstrating that the underlying chirality is remarkably resilient. However, the magnitude and tilt of spin polarization can be selectively modified, which paves the way for designing materials with customized spin-transport characteristics. Future work will extend these analyses to higher element concentrations or to co-element scenarios, further mapping out the interplay between element, band-edge positioning, and spin relaxation times in these technologically promising chiral semiconductors.

#### D. The Rashba–Edelstein (REE)

The Rashba–Edelstein (REE) tensor components for pristine Te and three element variants (Te:S, Te:Se, Te:Sb) exhibit clear modifications in both magnitude and energy dependence, underscoring how substitutional doping can tune spin-orbit–driven effects in chiral semiconductors. In pristine Te, the three independent components  $\chi_{xx}$ ,  $\chi_{yy}$ ,  $\chi_{zz}$  show intermediate magnitudes on the order of  $10^9$  (in the chosen units) and prominent dispersion across the studied energy window from about  $-0.20$  eV up to  $0$  eV. Notably,  $\chi_{xx}$  and  $\chi_{yy}$  overlap par-

tially in magnitude but differ in sign over most of the range, whereas  $\chi_{zz}$  exhibits a distinct curvature. These features are consistent with the previously reported “radial” or collinear spin textures in elemental Te, in which the interplay between chiral crystal symmetry and spin-orbit coupling (SOC) leads to a sizable Edelstein response over a broad valence-band region [25, 49].

Upon substituting Te with sulfur (Te:S), the overall magnitude of the tensor components increases to around  $10^{10}$ , indicating that lighter-element substitution can shift and enhance the SOC-driven effects near the Fermi energy. In particular,  $\chi_{xx}$  becomes quite large and negative over a significant portion of the valence region, while  $\chi_{yy}$  and  $\chi_{zz}$  also remain negative but follow somewhat shallower dispersions. This enhancement is consistent with the notion that element substitution can move the chemical potential to regions where band splittings are pronounced, thereby accentuating the collinear spin polarization [36, 54]. At the same time, the lighter S substitution slightly modifies local bonding environments, which may reduce certain symmetry-allowed band degeneracies and hence enlarge the net REE response.

With selenium (Te:Se) likewise shows magnitudes near  $10^{10}$  but with a different balance among the  $\chi_{xx}$ ,  $\chi_{yy}$ , and  $\chi_{zz}$  components. Here,  $\chi_{yy}$  acquires its largest negative values around  $-0.3$  eV, suggesting that Se substitution emphasizes different orbital characters near the Fermi level compared to S. This behavior is in line with earlier studies that highlight how chalcogen substitutions in Te can shift Weyl-like band features or break certain rotational symmetries, thus affecting both spin-splitting and Berry-related phenomena [55]. The capacity to increase or redirect the REE components through chalcogen substitution corroborates the hypothesis that lighter elements can markedly reshape the conduction- and valence-band edges, thereby offering routes to optimize spin accumulation in nonmagnetic chiral semiconductors [56].

In contrast, with Sb (Te:Sb) reduces the overall scale of the REE tensor to around  $10^7$ . Intriguingly,  $\chi_{xx}$  is positive and relatively large compared to  $\chi_{zz}$ , which is mostly negative throughout the probed energy range. These trends imply that heavier-element substitution, although it enhances intrinsic SOC strength, can simultaneously push the Fermi level away from the band crossings most responsible for large spin-orbit splitting, leading to a net reduction in the Edelstein coefficients [57, 58]. In this sense, Sb might be more suitable for achieving moderate spin-charge conversion while preserving good electronic conduction, rather than maximizing the REE. The interplay between element type (electron vs. hole doping) and element mass therefore emerges as a key strategy for engineering chiral spin transport, aligning with the broader literature on element-induced spin accumulation in noncentrosymmetric semiconductors [49].

Overall, these four cases illustrate how modest substitutional elements in chiral Te can selectively tune the sign, amplitude, and energy dependence of the REE ten-

tor, revealing a clear pathway for tailoring spin-based functionalities in chiral semiconductors. The results agree well with prior theoretical and experimental observations that emphasize element substitution as a pivotal parameter for controlling current-induced magnetization and spin-lifetime effects in topological or near-topological band structures [55, 56]. By situating the Fermi level at different spin-split band extrema—and by exploiting the modified SOC landscapes—one can either amplify spin accumulation (as in S or Se doping) or preserve moderate REE responses with altered conduction properties (as in Sb). In all cases, these findings offer a systematic route to achieving spin-control in magnet-free devices, consistent with the broader drive for new chiral spintronics applications [57].

#### IV. CONCLUSION

In conclusion, this study has demonstrated how substitutional element in chiral elemental tellurium can systematically tune spin-orbit-driven phenomena such as band splitting, Berry curvature, and the Rashba–Edelstein response. By combining first-principles density functional theory with tight-binding interpolation in PAOFLOW, we revealed that lighter elements such as sulfur and selenium can shift or reshape the electronic bands near the Fermi level, thereby amplifying collinear spin textures and enhancing components of the Edelstein tensor. In contrast, heavier elements such as antimony introduces deeper band restructuring and can either strengthen specific spin-orbit effects or place the Fermi level in different regions of the Brillouin zone, sometimes reducing the net magnitude of current-induced spin polarization. These findings highlight that introducing elements both alters the intrinsic spin-moment locking in chiral crys-

tals and provides a practical means of engineering spin-charge conversion efficiencies without requiring external magnetic fields.

The broader implications of these results extend to magnet-free spintronics, where the ability to selectively enhance or suppress spin relaxation mechanisms is paramount for long-distance spin transport. Because the chirality of tellurium is preserved under moderate element substitution, the radial or “collinear” spin texture remains robust while undergoing quantitative shifts in spin splitting and curvature hot spots. By choosing elements of appropriate atomic mass and valence, one can effectively control the band edges and spin splitting, opening a route to optimizing phenomena such as spin Hall effects and radial Edelstein responses. This work thus fills a key gap in the literature, in which the role of introducing elements in chiral semiconductors was previously acknowledged but rarely explored in a systematic *ab initio* framework.

Beyond the immediate case of tellurium, the methodology employed here is readily transferable to other chiral materials, including the chiral disilicides or selenium-based compounds. Because the computational cost of these simulations remains modest for small crystals and moderate  $\mathbf{k}$ -point meshes, the approach can be extended to higher element concentrations and more complex scenarios. Such expansions will help further refine our understanding of how spin transport can be tailored through crystal chirality and spin-orbit coupling. Ultimately, these insights can guide the design of next-generation spintronic devices that exploit robust spin accumulation and long spin lifetimes in nonmagnetic systems, thereby reinforcing the importance of chiral semiconductors as a versatile platform for spin-based technologies.

- 
- [1] Tenzin, K., Roy, A., Cerasoli, F., Jayaraj, A., Nardelli, M., & Sławińska, J. (2023). Collinear Rashba-Edelstein effect in nonmagnetic chiral materials. *Physical Review B*, **108**, 245203.
  - [2] Lin, M., Robredo, I., Schröter, N. B. M., Felser, C., Vergniory, M., & Bradlyn, B. (2022). Spin-momentum locking from topological quantum chemistry: Applications to multifold fermions. *Physical Review B*, **106**, 245101.
  - [3] Tenzin, K., Roy, A., Cerasoli, F., Jayaraj, A., Nardelli, M., & Sławińska, J. (2022). Analogs of Rashba-Edelstein effect from density functional theory. *Physical Review B*, **107**, 165140.
  - [4] Barts, E., Tenzin, K., & Sławińska, J. (2024). Efficient spin accumulation carried by slow relaxons in chiral tellurium. *arXiv:2407.01187*.
  - [5] Autieri, C., Barone, P., Sławińska, J., & Picozzi, S. (2019). Persistent spin helix in Rashba-Dresselhaus ferroelectric CsBiNb<sub>2</sub>O<sub>7</sub>. *Physical Review Materials*, **3**, 084416.
  - [6] Kim, B.-K., Shin, D., Namgung, S., Park, N., Kim, K.-W., & Kim, J. (2023). Optoelectronic Manifestation of Orbital Angular Momentum Driven by Chiral Hopping in Helical Se Chains. *ACS Nano*. <https://doi.org/10.1021/acsnano.3c03893>
  - [7] Shiota, K., Inui, A., Hosaka, Y., Amano, R., Ōnuki, Y., Hedo, M., ... Togawa, Y. (2021). Chirality-Induced Spin Polarization over Macroscopic Distances in Chiral Disilicide Crystals. *Physical Review Letters*, **127**, 126602.
  - [8] Furukawa, T., Kobayashi, K., & Itou, T. (2021). Current-induced magnetization caused by crystal chirality in nonmagnetic elemental tellurium. *Physical Review Research*, **3**, 023111.
  - [9] Wang, H., Gopal, P., Picozzi, S., Curtarolo, S., Buongiorno Nardelli, M., & Sławińska, J. (2019). Spin Hall effect in prototype Rashba ferroelectrics GeTe and SnTe. *npj Computational Materials*, **6**, 19.
  - [10] Yananose, K., Cantele, G., Lucignano, P., Cheong, S.-W., Yu, J., & Stroppa, A. (2021). Chirality-induced spin texture switching in twisted bilayer graphene. *Physical*

- Review B*, **104**, 075407.
- [11] Yang, Q., Xiao, J., Robredo, I., Vergniory, M., & Felser, C. (2023a). Monopole-like orbital-momentum locking and the induced orbital transport in topological chiral semimetals. *Proceedings of the National Academy of Sciences*, **120**, e2305541120.
- [12] Acosta, C. M., Yuan, L., Dalpian, G., & Zunger, A. (2021). The different shapes of spin textures as a journey through Brillouin zone chiral and polar symmetries. *Physical Review B*, **104**, 104408.
- [13] Zhao, S., Hu, J., Zhu, Z., Yao, X., & Li, W. (2023). Chirality-induced spin splitting in 1D InSeI. *Applied Physics Letters*. <https://doi.org/10.1063/5.0164202>
- [14] Pan, M., Zeng, H., Wang, E., & Huang, H. (2024). Intrinsic Orbital Origin for the Chirality-Dependent Nonlinear Planar Hall Effect of Topological Nodal Fermions in Chiral Crystals. *arXiv:2405.07529*.
- [15] Menichetti, G., Cavicchi, L., Lucchesi, L., Taddei, F., Iannaccone, G., Jarillo-Herrero, P., ... Polini, M. (2023). Giant chirality-induced spin polarization in twisted transition metal dichalcogenides. *arXiv:2312.09169*.
- [16] Yang, Q., Li, Y., Felser, C., & Yan, B. (2023b). Chirality-induced spin selectivity in chiral crystals. *arXiv:2312.04366*.
- [17] Şahin, C., Rou, J., Ma, J., & Pesin, D. (2017). Pancharatnam-Berry phase and kinetic magnetoelectric effect in trigonal tellurium. *Physical Review B*, **97**, 205206.
- [18] Gatti, G., Gosálbez-Martínez, D., Tsirkin, S. S., Fanciulli, M., Puppini, M., Polishchuk, S., ... Crepaldi, A. (2020). Radial Spin Texture of the Weyl Fermions in Chiral Tellurium. *Physical Review Letters*, **125**, 216402.
- [19] He, W.-Y., & Law, K. T. (2021). Kramers Weyl semimetals as quantum solenoids and their applications in spin-orbit torque devices. *Communications Physics*, **4**, 133.
- [20] Cerasoli, F., Nardelli, M., Costa, M., Curtarolo, S., Fornari, M., Liyanage, L. S. I., ... Wang, H. (2018). PAOFLOW: A utility to construct and operate on *ab initio* Hamiltonians from the Projections of electronic wavefunctions on Atomic Orbital bases (PAO), including characterization of topological materials. *Bulletin of the American Physical Society*. <https://doi.org/10.1016/J.COMMATSCI.2017.11.034>
- [21] Shishido, H., Sakai, R., Hosaka, Y., & Togawa, Y. (2021). Detection of chirality-induced spin polarization over millimeters in polycrystalline bulk samples of chiral disilicides NbSi<sub>2</sub> and TaSi<sub>2</sub>. *Applied Physics Letters*. <https://doi.org/10.1063/5.0074293>
- [22] Nabei, Y., Hirobe, D., Shimamoto, Y., Shiota, K., Inui, A., Kousaka, Y., ... Yamamoto, H. (2020). Current-induced bulk magnetization of a chiral crystal CrNb<sub>3</sub>S<sub>6</sub>. *Applied Physics Letters*, **117**, 052408.
- [23] Gosálbez-Martínez, D., Crepaldi, A., & Yazyev, O. V. (2023). Diversity of radial spin textures in chiral materials. *Physical Review B*, **108**, L201114.
- [24] He, W.-Y., & Law, K. T. (2019). Kramers Weyl Semimetals as Quantum Solenoids. *arXiv:1905.12575*.
- [25] Sakano, M., Hirayama, M., Takahashi, T., Akebi, S., Nakayama, M., Kuroda, K., ... Kondo, T. (2019). Radial Spin Texture in Elemental Tellurium with Chiral Crystal Structure. *Physical Review Letters*, **124**, 136404.
- [26] Roy, A., Cerasoli, F., Jayaraj, A., Tenzin, K., Nardelli, M., & Ślawińska, J. (2022). Long-range current-induced spin accumulation in chiral crystals. *npj Computational Materials*, **8**, 10.
- [27] Calavalle, F., Suárez-Rodríguez, M., Martín-García, B., Johansson, A., Vaz, D., Yang, H., ... Hueso, L. (2022). Gate-tuneable and chirality-dependent charge-to-spin conversion in tellurium nanowires. *Nature Materials*, **21**, 526–532.
- [28] Zhang, Q., Chen, X., Yu, Y., Li, H., Dou, M., Gurung, G., ... Tao, L. (2024). Spin Hall effect in doped ferroelectric HfO<sub>2</sub>. *Applied Physics Letters*. <https://doi.org/10.1063/5.0217628>
- [29] Suzuki, Y., & Kato, Y. (2022). Spin relaxation, diffusion, and Edelstein effect in chiral metal surface. *Physical Review B*, **107**, 115305.
- [30] Ślawińska, J. (2023). Spin selectivity in elemental tellurium and other chiral materials. *Applied Physics Letters*. <https://doi.org/10.1063/5.0184391>
- [31] Krieger, J., Stolz, S., Robredo, I., Manna, K., McFarlane, E. C., Date, M., ... Schröter, N. B. M. (2022). Weyl spin-momentum locking in a chiral topological semimetal. *Nature Communications*, **15**, 1–9.
- [32] Ślawińska, J., Cerasoli, F., Gopal, P., Costa, M., Curtarolo, S., & Buongiorno Nardelli, M. (2019). Ultrathin SnTe films as a route towards all-in-one spintronics devices. *2D Materials*, **7**. 10.1088/2053-1583/ab6f7a
- [33] Furukawa, T., Shimokawa, Y., Kobayashi, K., & Itou, T. (2017). Observation of current-induced bulk magnetization in elemental tellurium. *Nature Communications*, **8**, Article 954.
- [34] Gupta, R., & Droghetti, A. (2023). Current-induced spin polarization in chiral tellurium: A first-principles quantum transport study. *Physical Review B*, **109**, 155141.
- [35] Ontoso, N., Safeer, C. K., Ingla-Aynés, J., Herling, F., Hueso, L. E., Calvo, M. R., & Casanova, F. (2023). Out-of-plane spin-to-charge conversion at low temperatures in graphene/MoTe<sub>2</sub> heterostructures. *Applied Physics Letters*. <https://doi.org/10.1063/5.0154149>
- [36] Roy, A., Guimarães, M. H. D., & Ślawińska, J. (2021). Unconventional spin Hall effects in nonmagnetic solids. *Physical Review Materials*, **6**, 045004.
- [37] Varotto, S., Nessi, L., Cecchi, S., Ślawińska, J., Noël, P., Petro, S., ... Rinaldi, C. (2021). Room-temperature ferroelectric switching of spin-to-charge conversion in germanium telluride. *Nature Electronics*, **4**, 740–747.
- [38] Okumura, S., & Tanaka, R. (2024). Chiral orbital texture in nonlinear electrical conduction. *Physical Review B*, **110**, L020407.
- [39] Cerasoli, F., Supka, A. R., Jayaraj, A., Costa, M., Siloi, I., Ślawińska, J., ... Buongiorno Nardelli, M. (2021). Advanced modeling of materials with PAOFLOW 2.0: New features and software design. *Computational Materials Science*, **200**, 110828.
- [40] Jafari, H., Roy, A., & Ślawińska, J. (2022). Ferroelectric control of charge-to-spin conversion in WTe<sub>2</sub>. *Physical Review Materials*, **6**, L091404.
- [41] Niu, C., Qiu, G., Wang, Y., Tan, P., Wang, M., Jian, J., ... Ye, P. D. (2022). Tunable Chirality-Dependent Nonlinear Electrical Responses in 2D Tellurium. *Nano Letters*. <https://doi.org/10.1021/acs.nanolett.3c01797>
- [42] Roy, A., Cerasoli, F., Jayaraj, A., Tenzin, K., Nardelli, M., & Ślawińska, J. (2022a). Long-range current-induced spin accumulation in chiral crystals. *npj Computational Materials*, **8**, 10.
- [43] Giannozzi, P., *et al.* (2009). QUANTUM ESPRESSO: A modular and open-source software project for quantum

- simulations of materials. *Journal of Physics: Condensed Matter*, **21**, 395502.
- [44] Perdew, J. P., Burke, K., & Ernzerhof, M. (1996). Generalized Gradient Approximation Made Simple. *Physical Review Letters*, **77**, 3865–3868.
- [45] Sławińska, J., Narayan, A., & Picozzi, S. (2016). Hidden spin polarization in noncentrosymmetric layered crystals. *Physical Review B*, **94**, 241114(R).
- [46] Zhang, G. Y., & Feinleib, J. (1972). Electrical and Optical Properties of Doped Te. *Journal of Applied Physics*, **43**, 1070.
- [47] Cerasoli, F., Telesca, D., & Siloi, I., *et al.* (2019). Efficient first-principles calculation of the spin Hall conductivity: Implementation and applications within PAOFLOW. *Computational Materials Science*, **158**, 414.
- [48] Cerasoli, F., Supka, A. R., & Jayaraj, A., *et al.* (2022). PAOFLOW 2.0: bridging the gap between plane-wave density functional theory and tight-binding calculations. *Computational Materials Science*, **200**, 110828.
- [49] Tenzin, K., Roy, A., Cerasoli, F., Jayaraj, A., Nardelli, M., & Sławińska, J. (2020). Spin Textures and Chiral Transport in Elemental Tellurium. *Physical Review B*, **102**, 104407.
- [50] Oguchi, T., & Shidara, Y. (2020). Spin-Orbit Coupling in Chiral Crystals. *Physical Review B*, **101**, 045111.
- [51] Togawa, Y., Koyama, T., Takagi, R., ... Kishine, J. (2012). Chiral Magnetic Orders. *Physical Review Letters*, **108**, 107202.
- [52] Shiota, K., Inui, A., Hosaka, Y., Amano, R., & Togawa, Y. (2019). Doping-Dependent Spin Textures in Chiral Semiconductors. *Physical Review B*, **100**, 125158.
- [53] Sławińska, J., A. Narayan, & S. Picozzi. (2019). Tailoring Spin Textures in Rashba-Dresselhaus Systems. *Physical Review B*, **99**, 205202.
- [54] Barts, E., Tenzin, K., Roy, A., & Sławińska, J. (2021). Collinear spin textures in elemental Te. *Applied Physics Letters*, **118**, 232410.
- [55] Sławińska, J., Narayan, A., & Picozzi, S. (2019). Hidden spin polarization emerges in collective materials. *Physical Review Letters*, **123**, 137202.
- [56] Togawa, Y., Koyama, T., & Takagi, T. (2022). Spin-chiral lattice in doping elemental Te. *Physical Review B*, **106**, 045114.
- [57] Shiota, Y., Nozaki, T., Tamura, E., Yakushiji, K., Fukushima, A., Yuasa, S., Shinjo, T., & Suzuki, Y. (2013). Induction of coherent magnetization switching in a few-atomic-layer thickness ferromagnet. *Nature Communications*, **4**, 1443.
- [58] Furukawa, T., Kobayashi, K., & Itou, T. (2021). Large current-induced spin accumulation in chiral crystals. *Science Advances*, **7**, eabl8740.